RESEARCH ARTICLE

Macromolecular Chemistry and Physics
www.mcp-journal.de

Unveiling the Role of Compositional Drifts on the Tack of Pressure-Sensitive-Adhesives

*Anthony Arrowood, Morris Li, Mostafa Nassr, Nathaniel A. Lynd, and Gabriel E. Sanoja**

Pressure-sensitive-adhesives (PSAs) are pervasive in electronic, automobile, packaging, and biomedical applications due to their ability to stick to numerous surfaces without undergoing chemical reactions. These materials are typically synthesized by the free radical copolymerization of alkyl acrylates and acrylic acid, leading to an ensemble of polymer chains with varying composition and molecular weight. Here, reversible addition—fragmentation chain-transfer (RAFT) copolymerizations in a semi-batch reactor are used to tailor the molecular architecture and bulk mechanical properties of acrylic copolymers. In the absence of cross-links, the localization of acrylic acid toward the chain ends leads to microphase separation, creep resistance, and enhanced tack. However, in the presence of $Al(acac)_3$ crosslinker, the creep resistance remains unchanged and mostly the large-strain mechanical properties are affected. This behavior is attributed to microphase separation, but also to a change in the energy required to break physical associations, and untangle and elongate associative polymers to large deformations.

1. Introduction

Pressure-sensitive-adhesives (PSAs) are widespread in electronic, automobile, packaging, and biomedical applications as they instantaneously adhere to a variety of surfaces without undergoing chemical reactions.[1] Molecularly constituted of soft and dissipative polymer networks ($G' < 0.1$ MPa and $0.1 < \tan(\delta) < 1$ at 1 Hz),[2] these materials are typically produced by copolymerizing a set of monomers by chain growth copolymerization, and cross-linking the resulting polymers with, for example, electron acceptors like aluminum acetylacetonate.[3,4] Thus, PSAs are inherently inhomogeneous polymers, with chains that may compositionally drift due to differences in comonomer reactivity ratios, and copolymer mesophases that evolve as a result of chemical incompatibility and chain segregation.[5]

Over the past few decades, there have been some investigations focused on understanding the role of compositional inhomogeneities on the phase behavior and mechanical properties of copolymers. For the purposes of this work, three previous results are worth highlighting. The first is that gradient copolymers are not as segregated at mesoscopic length scales as block copolymers.[6–8] The second is that mechanical properties such as the glass transition breadth, ΔT_g, elastic modulus, and strain at break are notably affected by compositional gradients along the polymer chains.[9,10] And the third is that localizing the crosslinks near the center of the polymer chains, based on molecular dynamics simulations, decreases the average chain elongation before failure and, therefore, the network resistance to interfacial crack growth.[11] Overall, these results led us to hypothesize that compositional gradients along the polymer chains could serve as tool to leverage the molecular architecture and adhesive properties of acrylic copolymers.

To assess this hypothesis, we synthesized a series of symmetric and asymmetric poly(2-ethylhexyl acrylate-co-acrylic acid) copolymers with constant composition along the chains (88 mol.% EHA and 12 mol.% AA) but varying compositional gradient, L_x. The series was synthesized by conducting RAFT copolymerizations in a semi-batch reactor. The copolymers were cross-linked with aluminum acetylacetonate, $Al(acac)_3$, and their nanostructure and mechanical properties evaluated with a combination of X-ray scattering, linear amplitude oscillatory shear rheology, and probe-tack tests. The most interesting result is that gradients in composition along the polymer chains lead to dramatic changes in the adhesion energy or tack, but not on linear viscoelastic properties like the storage modulus and loss factor. Thus, this investigation unveils how to tune the large strain mechanical properties of soft and dissipative polymers through a combination of reversible deactivation radical copolymerizations (RDRPs) and reactor design.

2. Results and Discussion

2.1. Synthesis of Acrylic Copolymers with Varying Compositional Gradients along the Backbone

PSAs based on acrylic copolymers are among the most common.[12] They are typically manufactured by copolymerizing long-side chain 2-ethylhexyl acrylate (or n-butyl acrylate), short-side chain methyl acrylate, and electron donor acrylic acid, and cross-linking the resulting polymers with an electron acceptor like aluminum acetylacetonate.[3,4] Thus, these materials are very

A. Arrowood, M. Li, M. Nassr, N. A. Lynd, G. E. Sanoja
McKetta Department of Chemical Engineering
The University of Texas at Austin
Austin, TX 78712, USA
E-mail: gesanoja@che.utexas.edu

The ORCID identification number(s) for the author(s) of this article can be found under https://doi.org/10.1002/macp.202300249

DOI: 10.1002/macp.202300249

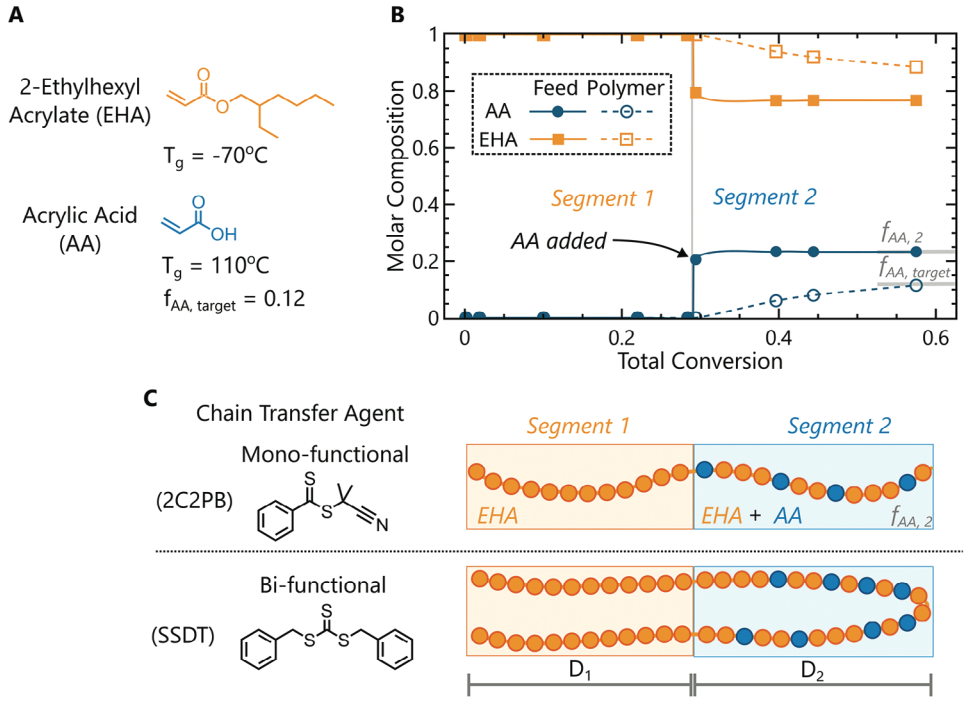

Figure 1. A) Comonomers used to synthesize acrylic copolymers. B) Representative feed and copolymer compositions before and after adding acrylic acid (AA). C) Compositional gradients in copolymers synthesized in the presence of 2-Cyano-2-propyl benzodithioate (2C2PB) and S,S-dibenzyltrithiocarbonate (SSDT) chain transfer agents.

versatile, having a tackiness, surface energy, and creep resistance that can be readily tuned through the monomer composition in the chain growth copolymerization.[13–15]

For the purposes of this work, there are two features of acrylic copolymerizations that are worth noting. The first is that they are uncontrolled, with chains that initiate, propagate, and rapidly terminate at low conversions. And the second is that they are random, with comonomers that have reactivity ratios, $r \approx 1$. These features led us to consider a RDRP like RAFT as a tool to synthesize copolymers with constant composition but varying compositional gradients along the chains. The strategy is inspired by the use of anionic copolymerizations to synthesize gradient and tapered copolymers.[8,16–18]

More specifically, we copolymerized 2-ethylhexyl acrylate (EHA, 88 mol.%) and acrylic acid (AA, 12 mol.%) in solution (30 wt.%) using ethyl acetate as a solvent. This formulation is typical of acrylic PSAs.[13–15,19,20] To control the kinetics of chain growth, we used either 2-Cyano-2-propyl benzodithioate (2C2PB) or S,S-dibenzyltrithiocarbonate (SSDT) as chain transfer agents (CTA). These CTAs afford narrow dispersities and well-defined molecular weights, and dictate the direction of chain growth.[21] The copolymerizations were conducted in a semi-batch reactor (i.e., adding the AA at different EHA conversions), leading to a series of copolymers with similar composition and molecular weight, $M_n \approx 100$ kDa, but varying compositional gradient along the chains. (see representative gradients in **Figure 1**, NMR spectra in Figures S1 and S2, Supporting Information and kinetics of copolymerization in Figure S3, Supporting Information).

Such compositional gradients can be quantified by considering the kinetics of chain growth copolymerization of EHA and AA. These comonomers have reactivity ratios close to one and, when polymerized within a batch reactor, lead to copolymer compositions like those of the feed (see Figure S4, Supporting Information):

$$N_A = f_A D \tag{1}$$

where N_A is the average number of AA comonomers in the copolymer chains, f_A the AA mole fraction, and D the degree of polymerization. Now, when the copolymerization is conducted in a semi-batch reactor and the AA is added at a degree of polymerization, D_1, the copolymer composition in the second segment is:

$$N_{A,2} = f_{A,2} D_2 \tag{2}$$

where $N_{A,2}$ is again the number of AA comonomers in the copolymer chains, $f_{A,2}$ the AA mole fraction, and D_2 the degree of polymerization after the addition of AA. For the copolymers synthesized in the batch and semi-batch reactors to have the same composition and molecular weight, the moles must be conserved according to:

$$D = D_1 + D_2 \tag{3}$$

$$N_A = N_{A,2} \tag{4}$$

Equations (1) to (4) can be used to obtain:

$$f_{A,2} = \frac{f_A}{L_x} \tag{5}$$

Table 1. Library of acrylic copolymers.

CTA	L_x	$f_{A,2}$ [a)]	f_A [b)]	Mn [kDa]	PDI
SSDT	1.0	0.13	0.13	95	1.53
SSDT	0.8	0.15	0.11	97	1.63
SSDT	0.5	0.22	0.11	98	1.62
SSDT	0.3	0.40	0.11	90	1.68
2C2PB	1.0	0.10	0.10	117	1.51
2C2PB	0.6	0.20	0.11	111	1.65
2C2PB	0.4	0.27	0.11	114	1.96

[a)] The average fraction of AA in the localized section of the copolymer, $f_{A,2}$, as measured by ^{1}H NMR (see details in Figure S2, Supporting Information). [b)] The average fraction of AA in the copolymer, f_A, as computed by Equation (5) and confirmed with ^{1}H NMR, methylating the acrylic acid comonomers with trimethylsilyldiazomethane to unveil a ^{1}H signal in the spectra (see Figure S1, Supporting Information). Mn and PDI as measured by GPC, using a refractive index detector calibrated against polystyrene standards.

where $L_x = 1 - D_1/D$ is the average fraction of the copolymer containing AA. Equation (5) is essential for synthesizing a series of acrylic copolymers of varying AA composition along the chain, as it relates the mixture composition, $f_{A,2}$, required after addition of AA to attain a copolymer with compositional gradient, L_x, and AA content, f_A. The limits of L_x are *1* and f_A and correspond to the cases of random and block copolymers, respectively.

A few points are worth emphasizing before discussing the structure-property relationships. The first is that the distribution of comonomers along the polymer chains can be readily tuned by conducting random copolymerizations in a semi-batch reactor. The second is that the copolymerizations should be terminated at relatively low conversions, 60%, to maintain control over the kinetics of chain growth. And the third is that, in this work, RAFT copolymerizations in semi-batch reactors were used to synthesize a series of acrylic copolymers with similar composition, $f_A = 0.12$ and molecular weight, $M_n \approx 100$ kDa but varying compositional gradient, L_x (see library of copolymers in **Table 1**, and more details on the kinetics of copolymerization in Section S2 Supporting Information).

2.2. Structure-Property Relationships of Acrylic Copolymer Melts

To unveil the role of compositional gradients on the adhesive properties of acrylic copolymers, we first note that, at room temperature, these materials are rubbery (see $T_g = -60^oC$ in Figure S5, Supporting Information), moderately entangled ($M_n/M_e = 3$), and with linear viscoelastic properties like those of conventional PSAs.[1] Specifically, the materials are soft ($G' \approx 0.01$ MPa at $\omega = 1$ rads^{-1}) and dissipative ($\tan(\delta) > 0.2$) when subjected to linear amplitude oscillatory shear rheology, with a resistance to creep that notably increases with the localization of AA along the polymer chains (see storage modulus and loss factor in **Figure 2**).

In terms of the large-strain mechanical properties, the compositional gradient, L_x, also plays an important role. When the AA comonomers are localized near the end of the copolymer chains, $L_x = 0.4$, the critical strain at which the stress drops after cavity nucleation and growth (i.e., after the peak in the stress-strain curve) increases from $\epsilon \approx 5$ to 8. This observation suggests that the material is able to nucleate fibrils that are more resistant to large deformations,[22] resulting in an increase in the adhesion energy, $W = h_0 \int \sigma \, d\epsilon$, from 50 to 140 Jm^{-2} (see **Figure 3**).

2.3. Structure—Property Relationships of Acrylic Copolymer Networks

While the acrylic copolymer melts are as soft and dissipative as conventional PSAs, they are not as creep resistant. As such, we cross-linked them with aluminum acetylacetonate, Al(acac)$_3$, (0.5 wt.% relative to the copolymer, or 22 mequiv. relative to AA) and turned them into soft polymer networks. Schematics of the chemical reaction and network architecture are presented in **Figure 4**.

Interestingly, cross-linking the acrylic melts with Al(acac)$_3$ leads to soft and dissipative networks, with a storage modulus, $G' \approx 0.01$ MPa, and loss factor, $\tan(\delta) \approx 1$, at a frequency, $\omega \approx 1$ rads^{-1}. However, the creep resistance is not as sensitive to the compositional gradient, L_x. We attribute this observation to the presence of Al-O associations and the hindered polymer dynamics. The linear viscoelastic properties of the random copolymers with $L_x = 1$ are also indistinguishable from each other, in agreement with the comparable composition and molecular weight of the precursor chains. (see **Figure 5**). We deem it worth noting that these acrylic copolymers fall within the Chang viscoelastic window, 0.01 to 100 rads^{-1}, often used to design PSAs.[2]

As opposed to the linear viscoelastic properties, the adhesive properties of the acrylic networks are notably influenced by L_x (see **Figure 6**). For an asymmetric gradient, the localization of AA near the chain ends leads to a change in the failure mechanism. Namely, when $L_x = 0.6$ or 0.4, the networks are unable to dissipate energy by nucleating and elongating stable fibrils, resulting in a decrease in the adhesion energy, W, from 210 to 30 Jm^{-2} (see **Figure 7**).

The symmetric case is rather similar, with the localization of AA near the center of the polymer chains also reducing adhesion over a range of L_x. Two behaviors are observed. The first is for $L_x = 1$ and 0.8, where the networks cavitate, the stress plateaus at 0.1 MPa, and there is fibrillation, energy dissipation, and elongation. And the second is for $L_x = 0.5$ and 0.3, where, again, the networks cavitate at the peak stress but the fibrils are too brittle and readily fail. The adhesion energy, W, decreases from 280 to 50 Jm^{-2} as $L_x \to f_A$. We deem it worth noting that the networks composed of symmetric and asymmetric copolymers should have the same adhesion energy, W, and their slight difference likely stems from their AA content, $f_A \approx 0.13$ and 0.10, respectively (see Table 1).

To rationalize this behavior, we examined the nanostructure of the acrylic copolymer melts and the networks through Small Angle X-Ray Scattering. After all, like in ionomers, the AA content is low, $f_A \approx 0.12$, and the chemical incompatibility with the EHA sufficient to drive microphase segregation.[23–25] The first interesting observation relates to the melts, which evolve higher-order peaks with the localization of the AA along the chains (see scattering profiles of $L_x = 0.4$ and $L_x = 0.3$ for the asymmetric and symmetric copolymers, respectively). These peaks are broader and more ill-defined than those of conventional block copolymers but indicative of some degree of long-range order. The microphase-separated nanostructure presumably consists of

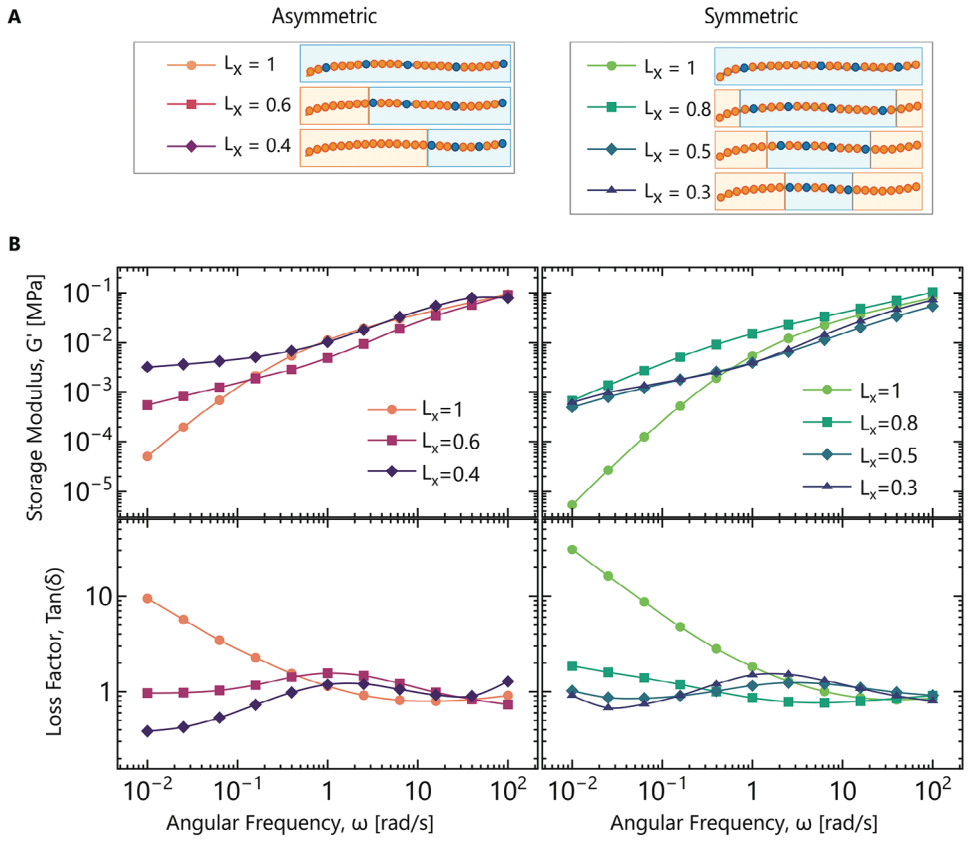

Figure 2. A) Schemes illustrating the compositional gradients in (left) asymmetric and (right) symmetric acrylic copolymers. B) Linear viscoelastic properties of (left) asymmetric and (right) symmetric copolymers reveal a considerable enhancement in the resistance to creep upon localization of the AA comonomers along the polymer chains.

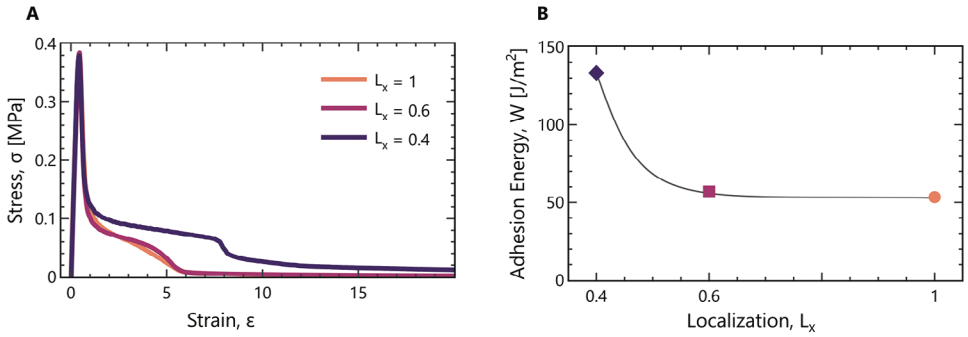

Figure 3. Adhesion of asymmetric copolymer melts. The (A) stress-strain curves during debonding illustrate an increase in the critical strain at which the stress completely drops. This increase is also reflected in (B) the adhesion energy, $W = h_0 \int \sigma d\epsilon$).

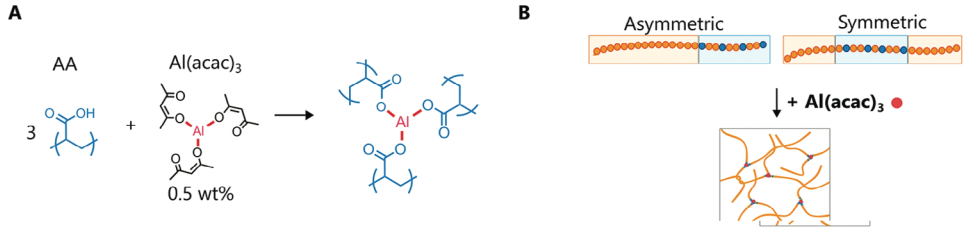

Figure 4. A) Chemical reaction between acrylic acid and aluminum acetylacetonate to cross-link the acrylic copolymers. B) The distribution of crosslinks for representative polymer chains having acrylic acid localized near the ends of the polymer chain for an asymmetric and symmetric chain.

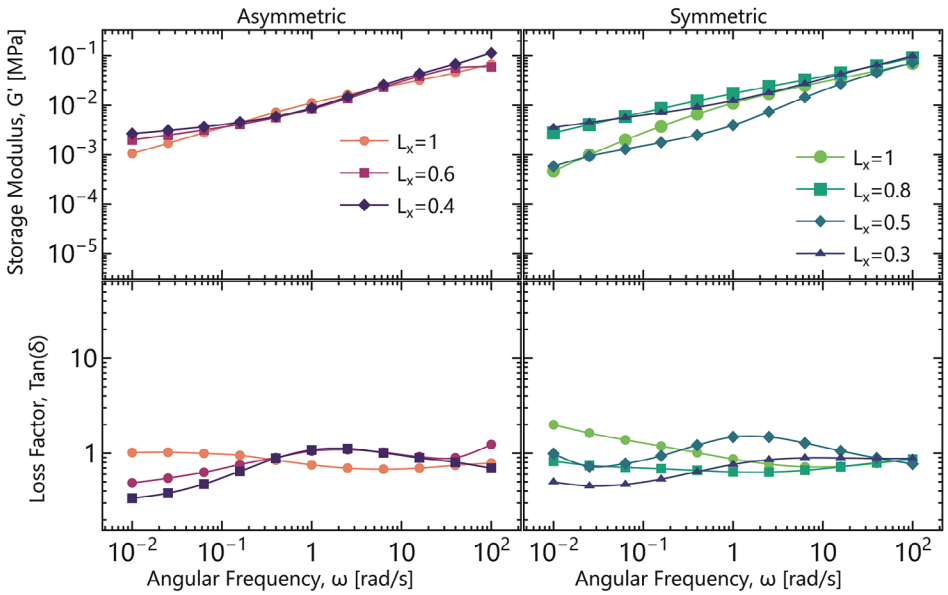

Figure 5. The small-strain rheological properties of the PSAs after cross-linking with $Al(acac)_3$. The storage modulus, G', (top) and the loss factor, $\tan(\delta)$ (bottom) for the networks resulting from (A) asymmetric and (B) symmetric copolymer chains. The storage modulus and loss factor appear rather insensitive to L_x

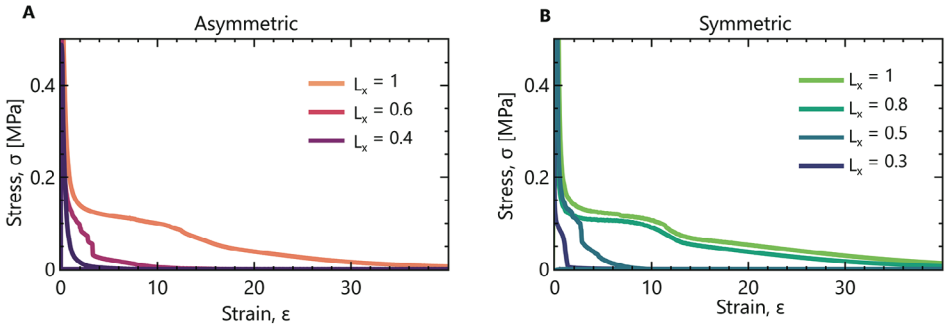

Figure 6. The stress–strain curves of the acrylic copolymers after cross-linking the (A) asymmetric and (B) symmetric chains with $Al(acac)_3$. The probe-tack tests were conducted at an initial strain rate of 1.2 s^{-1}

random poly(2-ethylhexyl acrylate-co-acrylic acid) domains embedded within a poly(2-ethylhexyl acrylate) matrix, leading to physical cross-linking, creep resistance, and enhanced tack. (see **Figure 8**).

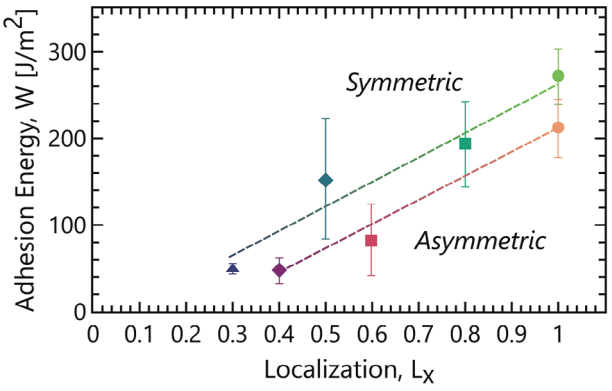

Figure 7. The adhesion energy ($W = h_0 \int \sigma d\epsilon$) of the acrylic networks as a function of the compositional gradient, L_x.

The acrylic networks also evolve broad, ill-defined, higher-order peaks as $L_x \rightarrow f_A$. Despite having similar scattering profiles to the acrylic melts, these materials now contain Al-O bonds that serve as physical cross-links. These cross-links hinder the dynamics of the polymer chains[26,27] and lead to linear viscoelastic properties that are largely unaffected by the segregation strength. However, the large-strain mechanical properties do change, with the chains being unable to untangle and elongate to their contour length and the nucleated fibrils having poor cohesive strength (see Figure 6). Hence, as $L_x \rightarrow f_A$, the acrylic networks become less tacky (see **Figure 9**).

A more intriguing observation relates to the ionomer-like regime, $L_x \rightarrow 1$, where the scattering profiles appear unchanged, but the adhesion energy, W, still depends on the compositional gradient along the chains. In this regime, the networks are heterogeneous at molecular length scales, and the Al-O associations presumably aggregate or cluster. Such clustering could impact

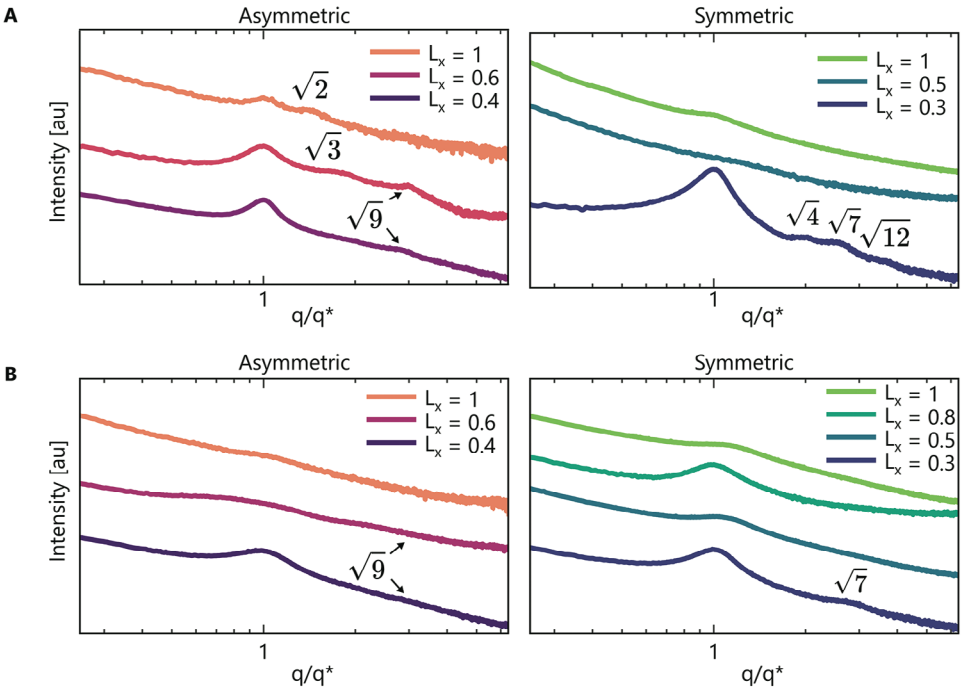

Figure 8. Small-angle X-ray scattering of the acrylic copolymers. Scattering profiles in the (A) melts reveal long-range order when the chains are (left) asymmetric and (right) symmetric. In the (B) networks, the presence of $Al(acac)_3$ reduces the long range order. However, the localization of AA along the chains still leads to some microphase separation.

the configuration of the polymer chains and their ability to untangle, elongate, and dissipate energy. Molecular dynamics simulations have suggested that localizing the AA monomers towards the center or the end of the polymer chains might hinder molecular self-diffusion and compromise adhesion,[11] and our experiments reveal that this is indeed the case.

3. Conclusion

We have investigated the role of compositional gradients on the adhesive properties of acrylic PSAs, and there are three points that we deem it worth highlighting. The first relates to the use of a RDRP such as RAFT in a semi-batch reactor, which allowed us to finely tune the compositional drift, L_x, in a family of acrylic polymers of similar composition, $f_A = 0.12$, and molecular weight, $M_n \approx 100$ kDa. Beyond affording polymers of narrow dispersity and well-defined molecular weight, the methodology provides a pathway to tailor the segregation strength and the molecular diffusivity of the polymer chains.

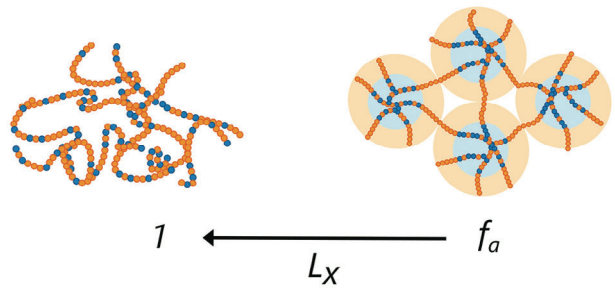

Figure 9. Microphase separation of gradient copolymers with the localization of AA along the polymer chains.

Prior to cross-linking, the compositional drift, L_x, drastically affects the nanostructure and mechanical properties of the acrylic melts. The localization of AA toward the center or the end of the polymer chains results in microphase separation, in agreement with the behavior of other block or tapered copolymers.[5,6,8] The melts likely assemble into a structure comprised of "stiff" poly(2-ethylhexyl acrylate-co-acrylic acid) domains embedded within a "soft" poly(2-ethylhexyl acrylate) matrix, which leads to linear viscoelastic properties like those of conventional PSAs. Specifically, the melts are soft, dissipative, and creep resistant, with an adhesion energy, $W = 130$ Jm^{-2}. However, unlike conventional PSAs, the acrylic melts are not cross-linked with a metal chelate such as $Al(acac)_3$ and they readily fail.

The impact of the compositional drift, L_x, on the acrylic networks is more intriguing. The localization of AA still leads to a microphase- separated structure, which does not influence the viscoelastic properties at low strains. However, what is particularly interesting is the effect of the compositional drift, L_x, on the large-strain mechanical properties. When $L_x \rightarrow f_A$, the networks microphase separate, are unable to dissipate energy, and cohesively fail under hydrostatic stress. However, when $L_x \rightarrow 1$, the networks are physically cross-linked like ionomers at molecular scales. The compositional drift, L_x, presumably affects the conformation of the polymer chains, as well as the energy required to break the Al-O associations and untangle and elongate the polymers.

Acrylic copolymers are commonly produced through free radical copolymerization, and are pervaded by gradients in composition and molecular weight. The copolymers are inhomogeneous

with intricate structure-property relationships. The use of RDRPs in a semi-batch reactor constitutes a strategy to unveil such relationships, and outline molecular designs for advanced materials with enhanced large-strain mechanical properties.

4. Experimental Section

Materials: Unless otherwise specified, all chemicals were used as received. 2-Ethyl-hexyl acrylate (EHA) was sourced from TCI; Acrylic acid (AA), 2-cyano-2-propyl benzodithioate (2C2PB), S,S-Dibenzyl trithiocarbonate (SSDT), aluminum acetylacetonate $Al(acac)_3$, Azobisisobutyronitrile (AIBN), and hydroquinone from Millipore-Sigma; and ethyl acetate, aluminum oxide, and methanol from VWR. Monomers 2EHA and AA were purified by eluting in aluminum oxide, and Azobisisobutyronitrile (AIBN) was recrystallized in methanol prior to use.

Synthesis of Acrylic Copolymers Melts: To 118 ml of ethyl acetate in a 250 ml round bottom flask, 165 mmol of 2EHA, 0.0936 mmol of chain transfer agent, and 0.01872 mmol of AIBN. This solution was deareated by sparging with nitrogen for 1 h and then transferred to a nitrogen-filled glovebox, whereby the solution was split evenly among four (4) 40 ml vessels each equipped with a magnetic stir bar. This allowed us to perform four (4) independent reactions in parallel. To vessel 1 (reaction 1), it added 5.56 mmol of acrylic acid. All vessels were heated to 60°C and stirred at 400RPM to initiate the reaction.

Aliquots were taken from each vessel during the reaction to monitor the conversion of 2EHA using ^{1}H NMR. While collecting the spectra, the copolymerization rate was decreased by holding the reactions unstirred at room temperature (≈25°C). The feed regimen - when and how much *AA* to add - for reactions 2, 3, and 4 was determined for each copolymer utilizing Equation (5) (see Section S2, Supporting Information).

The compositional drift (L_X) was targeted at ≈ 0.3, 0.5, and 0.7 for reactions 2, 3, and 4, respectively by choosing at which conversion to add *AA*. After *AA* was added to one of the vessels, the reactions were reheated to 80°C and 400RPM and another aliquot taken to determine the fraction of AA in the mixture.

After the conversion reached a target, 60%, the reactions were terminated by exposing to air. Thereafter, each reaction solution was precipitated in reagent alcohol three (3) times. The reactions with $L_x < \approx 0.4$ did not precipitate in alcohols and were extracted in water three (3) times. The polymers were redissolved in ethyl acetate, and dried overnight under vacuum at 80°C. They were subsequently lyophilized to remove any traces of water.

Synthesis of Acrylic Copolymers Networks: The acrylic melts were dissolved in ethyl acetate (0.1 gmL^{-1}), and cross-linked by adding a stock solution of $Al(acac)_3$ (1 gmL^{-1} in ethyl acetate) at 0.5 wt.% relative to the polymer. The resulting networks were stirred at 80°C for ≈2 h, concentrated in a rotary evaporator, and dried overnight in vacuum at 80°C. Based on estimates of the overlap concentration (0.01 gmL^{-1}), the melts were cross-linked in the concentrated regime.

Molecular and Thermomechanical Characterization: The molecular weight of the polymers was determined by Gel Permeation Chromatography (GPC), eluting with tetrahydrafuran over a T6000M column (Malvern Panalytical), and measuring the refractive index with a detector calibrated against polystyrene standards.

The glass transition temperature, T_g, was determined by Differential Scanning Calorimetry (DSC 250 TA Instruments Inc.) using the midpoint method, scanning three (3) times from -90 to 200 °C at 1 °Cmin^{-1}.

Rheological and Adhesive Testing: The polymers were placed between two (2) 36 µm thick non-stick silicone release liners (Drytac Inc.). With the PSAs in-between the sheets, the outside surfaces of the liners were heated to 80 °C and the sheet-PSA-sheet laminates pressed under a film coater of gap set to a desired thickness. The resulting PSAs were homogeneous, and stored at room temperature until use.

Specimens for rheology were prepared by die cutting the PSA laminates into 8mm diameter circles. The linearly viscoelastic properties, G' and $\tan(\delta)$, were determined in a TA Instruments HR2 Hybrid Rheometer; using an 8 mm probe equilibrated at 30 °C, and applying an oscillatory shear strain of 1% at frequencies ranging from 0.01 to 100 $rads^{-1}$.

Specimens for probe-tack tests were prepared by die cutting the PSA laminates into disks of 8 or 12 mm diameter. The tests were conducted in an Instron 34TM5 tensile-tester equipped with a 100 N load cell and affixed with a stainless steel probe having the same diameter of the disks. The PSA films were adhered to the probe, and compressed onto a glass or stainless steel substrate at a velocity of 10 μms^{-1} until reaching a compressive force of 50 N. Thereafter, the probe was retracted at a constant velocity of 100 μms^{-1}, and the resulting force-displacement curves were used to determine the stress, $\sigma = F/A$, strain, $\epsilon = (h - h_0)/h_0$, and adhesion energy, $W = h_o \int_0^{\epsilon_{max}} \sigma(\epsilon) d\epsilon$. Here, h_0 is the initial thickness, and A the cross-sectional area of the probe, $A = \pi D^2/4$. The stress-stretch curves and adhesion energies were mostly unaffected by substrate and probe diameter.

Small Angle X-Ray Scattering: Specimens for Small Angle X-ray Scattering were prepared by adhering PSA films onto circular washers. Scattering patters were collected at the Soft Matter Interfaces Beamline (12-ID) of the National Synchrotron Light Source II at Brookhaven National Laboratory. The X-ray source had an energy of 16.1 keV. The sample-to-detector distance was 9.2 m. The 2D scattering patterns were azimuthally integrated to generate 1D scattering profiles.

Supporting Information

Supporting Information is available from the Wiley Online Library or from the author.

Acknowledgements

This work was funded by the University of Texas at Austin, and used the Soft Matter Interfaces Beamline (12-ID) of the National Synchrotron Light Source II, a U.S. Department of Energy (DOE) Office of Science User Facility operated for the DOE Office of Science by Brookhaven National Laboratory under Contract No. DE-SC0012704. N.A.L. acknowledged support from the National Science Foundation (CHE-2004167).

Conflict of Interest

The authors declare no conflict of interest.

Data Availability Statement

The data that support the findings of this study are available from the corresponding author upon reasonable request.

Keywords

acrylic PSAs, adhesion science, block copolymer self-assembly, RAFT copolymerizations

Received: July 15, 2023
Revised: October 20, 2023
Published online: November 9, 2023

[1] C. Creton, *MRS Bull.* **2003**, *28*, 434.
[2] E. P. Chang, *J. Adhes.* **1991**, *34*, 189.
[3] Z. Czech, *J. Adhes. Sci. Technol.* **2007**, *21*, 625.

[4] Z. Czech, M. Wojciechowicz, *Eur. Polym. J.* **2006**, *42*, 2153.
[5] F. S. Bates, G. H. Fredrickson, *Annu. Rev. Phys. Chem.* **1990**, *41*, 525.
[6] K. R. Shull, *Macromolecules* **2002**, *35*, 8631.
[7] M. D. Lefebvre, M. Olvera de la Cruz, K. R. Shull, *Macromolecules* **2004**, *37*, 1118.
[8] N. Singh, M. S. Tureau, T. H. Epps III, *Soft Matter* **2009**, *5*, 4757.
[9] R. Lach, R. Weidisch, K. Knoll, *J. Polym. Sci., Part B: Polym. Phys.* **2005**, *43*, 429.
[10] M. M. Mok, J. Kim, C. L. H. Wong, S. R. Marrou, D. J. Woo, C. M. Dettmer, S. T. Nguyen, C. J. Ellison, K. R. Shull, J. M. Torkelson, *Macromolecules* **2009**, *42*, 7863.
[11] K. Jin, D. López Barreiro, F. J. Martin-Martinez, Z. Qin, M. Hamm, C. W. Paul, M. J. Buehler, *Polymer* **2018**, *154*, 164.
[12] C. Creton, M. Ciccotti, *Rep. Prog. Phys.* **2016**, *79*, 046601.
[13] S. D. Tobing, A. Klein, *J. Appl. Polym. Sci.* **2001**, *79*, 2230.
[14] A. Lindner, B. Lestriez, S. Mariot, C. Creton, T. Maevis, B. Lühmann, R. Brummer, *J. Adhes.* **2006**, *82*, 267.
[15] A. Arrowood, M. A. Ansari, M. Ciccotti, R. Huang, K. M. Liechti, G. E. Sanoja, *Soft Matter* **2023**, *19*, 6088.
[16] K. Knoll, N. Nießner, *Macromol. Symp.* **1998**, *132*, 231.
[17] P. Hodrokoukes, G. Floudas, S. Pispas, N. Hadjichristidis, *Macromolecules* **2001**, *34*, 650.
[18] S. Jouenne, J. A. González-León, A.-V. Ruzette, P. Lodefier, S. Tencé-Girault, L. Leibler, *Macromolecules* **2007**, *40*, 2432.
[19] R. Villey, C. Creton, P.-P. Cortet, M.-J. Dalbe, T. Jet, B. Saintyves, S. Santucci, L. Vanel, D. J. Yarusso, M. Ciccotti, *Soft Matter* **2015**, *11*, 3480.
[20] P. Karnal, P. Roberts, S. Gryska, C. King, C. Barrios, J. Frechette, *ACS Appl. Mater. Interfaces* **2017**, *9*, 42344.
[21] S. Perrier, *Macromolecules* **2017**, *50*, 7433.
[22] H. Lakrout, P. Sergot, C. Creton, *J. Adhes.* **1999**, *69*, 307.
[23] D. J. Yarusso, S. L. Cooper, *Macromolecules* **1983**, *16*, 1871.
[24] A. Eisenberg, B. Hird, R. B. Moore, *Macromolecules* **1990**, *23*, 4098.
[25] R. A. Register, *Macromolecules* **2020**, *53*, 1523.
[26] L. Leibler, M. Rubinstein, R. H. Colby, *Macromolecules* **1991**, *24*, 4701.
[27] Z. Zhang, Q. Chen, R. H. Colby, *Soft Matter* **2018**, *14*, 2961.